Lipid transporter TMEM24/C2CD2L is a Ca^{2+}-regulated component of ER–plasma membrane contacts in mammalian neurons

Elizabeth Wen Sun[a,b,c,d], Andrés Guillén-Samander[a,b,c,d], Xin Bian[a,b,c,d], Yumei Wu[a,b,c,d], Yiying Cai[a,b,c,d], Mirko Messa[a,b,c,d,1,2], and Pietro De Camilli[a,b,c,d,e,1]

[a]Department of Neuroscience, Yale University School of Medicine, New Haven, CT 06510; [b]Department of Cell Biology, Yale University School of Medicine, New Haven, CT 06510; [c]Howard Hughes Medical Institute, Yale University School of Medicine, New Haven, CT 06510; [d]Program in Cellular Neuroscience, Neurodegeneration, and Repair, Yale University School of Medicine, New Haven, CT 06510; and [e]Kavli Institute for Neuroscience, Yale University School of Medicine, New Haven, CT 06510

Contributed by Pietro De Camilli, January 14, 2019 (sent for review December 4, 2018; reviewed by Thierry Galli and Michael M. Tamkun)

Close appositions between the endoplasmic reticulum (ER) and the plasma membrane (PM) are a general feature of all cells and are abundant in neurons. A function of these appositions is lipid transport between the two adjacent bilayers via tethering proteins that also contain lipid transport modules. However, little is known about the properties and dynamics of these proteins in neurons. Here we focused on TMEM24/C2CD2L, an ER-localized SMP domain containing phospholipid transporter expressed at high levels in the brain, previously shown to be a component of ER–PM contacts in pancreatic β-cells. TMEM24 is enriched in neurons versus glial cells and its levels increase in parallel with neuronal differentiation. It populates ER–PM contacts in resting neurons, but elevations of cytosolic Ca^{2+} mediated by experimental manipulations or spontaneous activity induce its transient redistribution throughout the entire ER. Dissociation of TMEM24 from the plasma membrane is mediated by phosphorylation of an array of sites in the C-terminal region of the protein. These sites are only partially conserved in C2CD2, the paralogue of TMEM24 primarily expressed in nonneuronal tissues, which correspondingly display a much lower sensitivity to Ca^{2+} elevations. ER–PM contacts in neurons are also sites where Kv2 (the major delayed rectifier K^+ channels in brain) and other PM and ER ion channels are concentrated, raising the possibility of a regulatory feedback mechanism between neuronal excitability and lipid exchange between the ER and the PM.

SMP domain | lipid-transfer protein | potassium channel | extended synaptotagmin | VAP

The endoplasmic reticulum (ER) is a subcellular compartment with a multiplicity of functions, including synthesis of most membrane lipids. From the ER, lipids can be transported to all other membranes of the secretory and endocytic pathways via vesicular (or tubular) carriers. Conversely, lipid metabolites can return to the ER for metabolic recycling via this traffic. Vesicular transport alone, however, is not sufficient to generate and maintain the heterogeneity in lipid composition of different membranes of eukaryotic cells (1, 2). It also cannot account for the transport of lipids to organelles not connected to the exo-endocytic endomembrane system, such as mitochondria. Thus, lipid exchange between the ER and other membranes also occurs via lipid-transport proteins that can extract lipids from a bilayer, shield them from the aqueous environment of the cytosol in a hydrophobic cavity, and deliver them to another bilayer (3). Several recent studies have shown that much of this lipid transport occurs at sites of close contact (not leading to fusion) between membranes, as the proteins involved also function as tethers between the two membranes (4–7).

One class of lipid-transport modules found in intracellular proteins that function at membrane contact sites are SMP (synaptotagmin-like, mitochondrial and lipid-binding protein) domains (8–11). These domains represent a branch within the superfamily of TULIP (tubular lipid-binding) domains that comprise members found both in intracellular and extracellular proteins (12). SMP domain-containing proteins are present at contacts of the ER with either mitochondria (11, 13), the plasma membrane (PM) (8, 14, 15), or the Golgi complex (16). One such protein is TMEM24 (also called C2CD2L), which localizes at ER–PM contact sites. TMEM24 is anchored to the ER membrane via an N-terminal transmembrane span, which is followed by the SMP domain, a C2 domain, and a highly conserved, low-complexity and predominantly basic C-terminal region (CTR), which is the PM binding region (Fig. 1*A*). Its SMP domain harbors glycerolipids, with a bias toward inositol phospholipids (15). TMEM24 is primarily expressed in brain and in cells with neuron-like properties, such as pancreatic endocrine cells (15, 17). Studies of TMEM24 in pancreatic β-cells and of exogenously expressed tagged-TMEM24 in fibroblasts demonstrated that it is predominantly bound to the PM at rest and reversibly dissociates from it upon Ca^{2+}-dependent phosphorylation of its CTR (15). Properties of TMEM24 in neurons have not been explored so far.

Contacts between the ER and the PM are abundant in neurons and particularly large in cell bodies, where micrometer-sized ER

Significance

It is well established that the cross-talk between the plasma membrane (PM) and the endoplasmic reticulum (ER) plays an important role in neuronal signaling. Until recently, this cross-talk was thought to be mediated primarily by soluble second messengers, such as Ca^{2+} and IP3, although it has long been known that tight appositions between the ER and the PM occur in all cells and are abundant in neurons. Investigations of the proteins that populate these contacts are shedding new light on feedback regulatory mechanisms between the two membranes. The present study identifies the phospholipid transporter TMEM24/C2CD2L as a regulated component of ER–PM contacts in neurons and suggests that lipid transfer between the two bilayers participates in the control of neuronal signaling.

Author contributions: E.W.S., A.G.S., X.B., Y.C., M.M., and P.D.C. designed research; E.W.S., A.G.S., X.B., Y.W., Y.C., and M.M. performed research; E.W.S., A.G.S., X.B., M.M., and P.D.C. analyzed data; and E.W.S., A.G.S., X.B., M.M., and P.D.C. wrote the paper.

Reviewers: T.G., Institute of Psychiatry and Neurosciences of Paris; and M.M.T., Colorado State University.

The authors declare no conflict of interest.

[1]To whom correspondence may be addressed. Email: messa.mirko@gmail.com or Pietro.decamilli@yale.edu.

[2]Present address: Department of Neuroscience, Novartis Institutes for BioMedical Research, Cambridge, MA 02139.

This article contains supporting information online at www.pnas.org/lookup/suppl/doi:10.1073/pnas.1820156116/-/DCSupplemental.

Published online February 28, 2019.

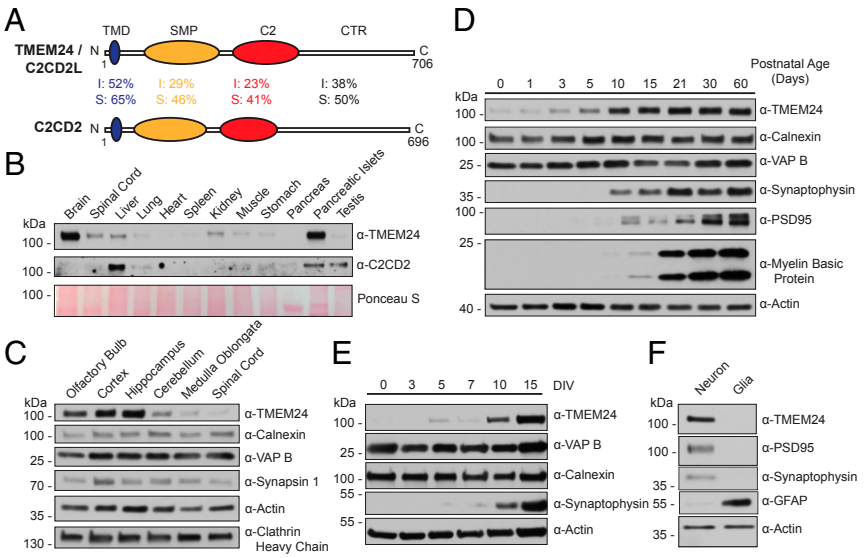

Fig. 1. Expression pattern of TMEM24 and C2CD2 in mammalian tissues. (*A*) Domain organization of human TMEM24/C2CD2L and C2CD2. Amino acid identity (I) and similarity (S) are indicated for the various domains. (*B*) Immunoblots showing protein expression of TMEM24 and C2CD2 in several adult mouse tissues. TMEM24 is highly expressed in the brain and pancreatic islets. Note that it migrates at an apparent higher molecular mass (>100 kDa) than its predicted size (76 kDa). Ponceau S staining show loading. (*C*) Immunoblots of adult mouse brain regions showing that TMEM24 is highly expressed in the forebrain but less in the hindbrain, while other proteins, including ER proteins (VAPB and calnexin), shown for comparison, are more evenly expressed. (*D*) Immunoblots of brain cerebral cortex lysates collected from postnatal mice at different ages showing that TMEM24 expression increases with neuronal and synaptic maturation. (*E*) Immunoblots of primary cultured neurons demonstrating selective expression of TMEM24 upon neuronal maturation. (*F*) Immunoblots of glial-free cortical neuronal culture (18 DIV) and glial cell culture lysates showing that TMEM24 is predominantly expressed in neurons relative to glia. GFAP is used as glial cell marker.

cisternae (often with a very narrow lumen) closely apposed to the PM (distance less than 30 nm) can cover ∼10% of this membrane (18). However, the molecular composition of such contacts remains poorly explored. Most endogenous components investigated so far are proteins directly or indirectly implicated in ion transport. They include voltage-dependent Ca^{2+} and K^+ channels (19, 20) in the PM and the ryanodine receptor (21), its associated factor junctophilin (22), and STIM (23, 24) in the ER. Very recently, the ER protein VAP, an interactor of several lipid-metabolizing enzymes and lipid-transport proteins, was also shown to be concentrated at neuronal ER–PM contacts, where it mediates the recruitment of Kv2 channels (25–27). The localization to the same sites of proteins with a role in lipid metabolism and transport would point to an interplay between lipid dynamics and neuronal signaling/excitability. While several such proteins are expressed in neurons, generally little is known about their localization and dynamics. Here we have investigated the expression, localization, and dynamics in the nervous system of TMEM24. Our results identify TMEM24 as a highly dynamic component of neuronal ER–PM contacts. We identify a polybasic amino acid stretch at the C terminus of its CTR as the key determinant of its association with the PM at rest and show that phosphorylatable serines in this stretch are responsible for its shedding in response to a variety of pharmacological and physiological manipulations leading to Ca^{2+} elevation. Accordingly, the TMEM24 paralog C2CD2 (Fig. 1*A*), which has a different tissue distribution from TMEM24 and is not enriched in the brain, lacks these serines, as well as Ca^{2+} regulation of its ER–PM tethering function. Collectively our results point to a role of TMEM24 at the intersection of lipid transport and neuronal signaling/excitability.

Results

TMEM24 Is Enriched in Neurons and Its Expression Correlates with Neuronal Maturation. A survey of the expression of TMEM24 in different mouse tissues by Western blotting confirmed that TMEM24 is expressed at particularly high concentration in the brain and in pancreatic islets (Fig. 1*B*) (17). Within the nervous system, TMEM24 is preferentially expressed in the fore- and midbrain over the hindbrain and the spinal cord (Fig. 1*C*). This difference contrasts the more even distribution of other neuronal proteins, such as synapsin and clathrin, as well as of other ER proteins, such as calnexin and VAPB, indicating that the enrichment of TMEM24 in the anterior regions of the brain does not simply reflect ER abundance. Furthermore, levels of TMEM24 in the brain strongly increase with postnatal development, while levels of calnexin and VAPB do not show a major change (Fig. 1*D*). This increase parallels, although does not precisely overlap with, the increase in the levels of proteins that mark synaptogenesis (PSD95 and synaptophysin) and myelination (myelin basic protein) (Fig. 1*D*). A rough correlation between brain maturation and expression of TMEM24, but not with expression of housekeeping ER proteins, was also observed in primary neuronal cultures (Fig. 1*E*). These findings point to a specific role of TMEM24 in the function of the mature neurons. Analysis of total lysates from primary cultures of glial cells and glia-free cortical neurons [28 d in vitro (DIV)] showed that TMEM24 is expressed predominantly by neurons (Fig. 1*F*), a finding that was confirmed by quantitative PCR measurement of the abundance of TMEM24 mRNA in neurons and glial cells. TMEM24 mRNA expression in neurons is 2.26 ± 0.26-fold higher than in glial cells.

TMEM24 Is Enriched at ER–PM Contact Sites in Neurons. The subcellular targeting of TMEM24 within nerve cells was assessed by expressing TMEM24-EGFP (enhanced green fluorescent protein) in hippocampal neuronal cultures. Confocal microscopy of equatorial regions of neuronal cell bodies demonstrated that TMEM24-EGFP primarily localized at hot spots in the cortical region of the cell (Fig. 2 *A* and *B*). A weaker signal was detected throughout the cytoplasm, which reflects ER localization, as shown by the ER marker GFP-Sec61β (Fig. 2*A*, see also ref. 15). The intensity of the peripheral hot spots relative to the signal

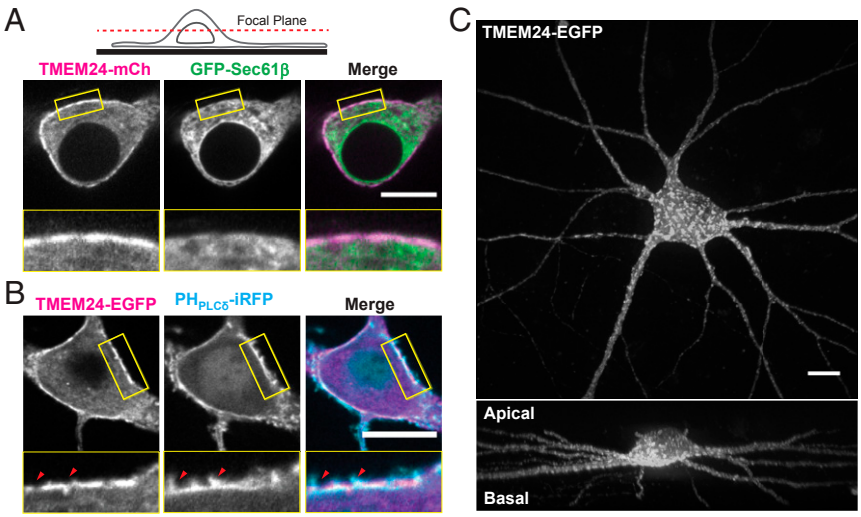

Fig. 2. TMEM24 is concentrated at ER–PM contact sites in primary culture of hippocampal neurons. (*A*) Representative confocal images of cultured hippocampal neurons (11 DIV) cotransfected with TMEM24-mCh and the ER marker EGFP-Sec61β. A schematic representation of the focal plane is shown (*Upper*). *Insets* (see rectangles) highlight the selective concentration of TMEM24-mCh relative to EGFP-Sec61β in peripheral patches. (Scale bar, 10 μm.) (*B*) Representative confocal images of cultured hippocampal neurons (16 DIV) cotransfected with TMEM24-EGFP and the PI(4,5)P_2 marker $PH_{PLC\text{-}\delta}$-iRFP. *Insets* (see rectangles) highlight that large patches of TMEM24-EGFP colocalize with the PI(4,5)P_2 probe, used here as a PM marker, but are absent from PM protrusions (arrowheads). (Scale bar, 10 μm.) (*C*) *En face* view of a 3D rendering from serial confocal sections of a cultured hippocampal neuron (14 DIV) transfected with TMEM24-EGFP. TMEM24-EGFP appears as bright patches throughout the somatodendritic regions of the neuron (*Upper*). Orthogonal view of the 3D reconstruction shows the preferential accumulation of TMEM24-EGFP at the basal face of the neuron nearest to the substrate (*Lower*). (Scale bar, 10 μm.) (Magnification: *Insets*, 2.5×.)

throughout the ER was somewhat variable among different neurons, due—at least in part—to level of expression. The patchy localization in the cortical regions of the cells was consistent with an enrichment of TMEM24-EGFP at ER–PM contact sites, as observed in insulinoma cells or transfected HeLa and COS7 cells (15). Patches were the largest in cell bodies (Fig. 2*C*, *Upper*, and Movie S1), where ER–PM contacts are known to be larger than in neuronal processes (28), with a preferential accumulation on the basal surface of neurons (the portion in contact with the substrate) (Fig. 2*C*, *Lower*). However, smaller patches were also clearly detectable in dendrites (Fig. 2*C*) and, less prominently, in axon initial segments (*SI Appendix*, Fig. S1; see also Fig. 7*A*). Only faint TMEM24-EGFP fluorescence was detectable throughout axons beyond the axon initial segment, so that it was not clear whether the protein was localized at ER–PM contact sites in axons as well (*SI Appendix*, Fig. S1).

If TMEM24 functions as a tether between the ER and the PM, its overexpression would be expected to expand areas of ER–PM contacts. Accordingly, analysis by conventional electron microscopy of neurons expressing TMEM24-EGFP in addition to endogenous TMEM24 revealed that both number and length of ER–PM appositions in perikarya and dendrites were increased (Fig. 3).

In some cells, patches of TMEM24-EGFP on the surface apposed to the substrate had a ring-like shape (*SI Appendix*, Fig. S2*A*, *Upper*). Confocal imaging perpendicular to the substrate revealed that the center of these rings coincided with infolding of

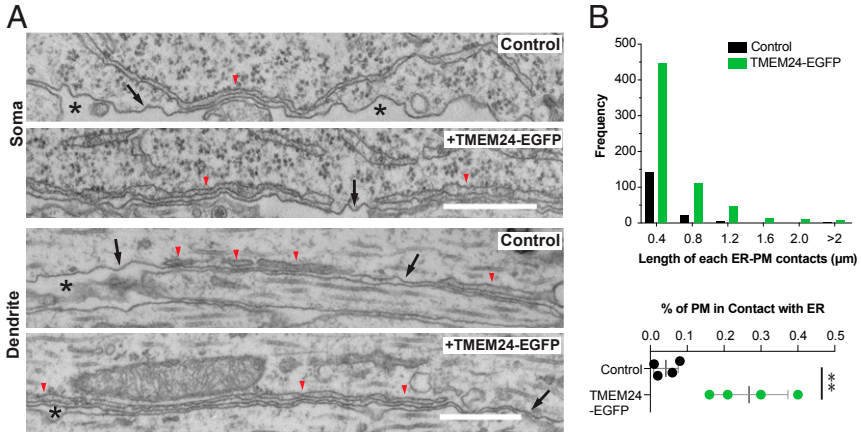

Fig. 3. TMEM24 overexpression increases areas of apposition of the ER with the PM in primary neuronal cultures. (*A*) Representative electron micrographs from soma and dendrites of control cultured cortical neurons (9 DIV) and neurons transfected with TMEM24-EGFP identified by correlative light electron microscopy (*Materials and Methods*). The PM is indicated by arrows and ER elements apposed to it are indicated by arrowheads. The length of ER–PM appositions is greater upon TMEM24-EGFP overexpression. Asterisks indicate extracellular space. (Scale bar, 500 nm.) (*B*) Morphometric analysis of EM micrographs shown as a distribution of lengths of individual ER–PM appositions (*Upper*) and as the average percentage of PM in contact with ER per cell (*Lower*). Four cells identified by correlative light electron microscopy were analyzed for each condition (total PM length quantified per condition = 768 μm). Data are represented as mean ± SD $n = 4$, $t(6) = -4.066$, $^{**}P = 0.0066$ (two-tailed, unpaired *t* test).

the PM with a rim of fluorescence at their edge (*SI Appendix*, Fig. S2*A*, *Lower*). Accordingly, inspection of these invaginations by EM in sections parallel to, and close to the substrate revealed ER–PM apposition at their edges and showed that the length of these appositions was increased in TMEM24-EGFP–expressing cells relative to WT cells. (*SI Appendix*, Fig. S2*B*).

To confirm that the localization of TMEM24-EGFP observed in neurons is not the result of the expression of an exogenous protein, the EGFP cDNA sequence was inserted "in frame" at the C terminus of the TMEM24 locus in a human neuroblastoma IMR32 cell line to induce expression of a tagged endogenous protein (endo–TMEM24-EGFP) (*SI Appendix*, Fig. S3). PCR-based analysis of DNA from these cells demonstrated the expected insertion of the EGFP sequence and absence of the corresponding WT sequence (Fig. 4*A*). Western blotting of cell homogenates for TMEM24 confirmed replacement of the endogenous band with another band at the expected higher molecular weight. While the difference in the intensity of the WT TMEM24 and endo–TMEM24-EGFP bands remains unexplained, anti-GFP immunoprecipitation followed by anti-TMEM24 Western blot confirmed the identity of the higher band as endo–TMEM24-EGFP (Fig. 4*B*). Inspection of these cells by confocal microscopy showed that endo–TMEM24-EGFP was primarily concentrated in peripheral cortical patches. Furthermore, upon exogenous expression of TMEM24 fused to a Halo-tag (TMEM24-Halo) (29), Halo and EGFP signals precisely colocalized, proving that the localization of exogenous TMEM24 reflects the endogenous localization of the protein (Fig. 4*C*). When knockin IMR32 cells were treated with BrdUrd to induce neuron-like differentiation (30), spots of endo–TMEM24-EGFP were observed both in the soma and in neurites (Fig. 4*D*).

Neuronal Depolarization and NMDA Receptor Stimulation Trigger Ca^{2+}-Dependent Shedding of TMEM24 from ER–PM Contacts. Our previous studies of nonneuronal cells revealed that the localization of TMEM24 is regulated by Ca^{2+}. Release of Ca^{2+} from intracellular stores, either by incubation of cells with thapsigargin (to inhibit the ER Ca^{2+} pump with a resulting activation of Store-Operated-Ca^{2+}-Entry) (31), or by stimulation with carbachol [to stimulate IP3 (inositol triphosphate) production] (32), induced a transient dissociation of TMEM24 from the PM due to phosphorylation of its CTR (15). Thus, we assessed the impact of stimulations that enhance cytosolic Ca^{2+} on the localization of TMEM24-EGFP in hippocampal neurons in primary culture (DIV 11–15).

While TMEM24-EGFP was concentrated at cortical patches at rest, it rapidly (within tens of seconds) redistributed to the reticular ER upon depolarization with 15 mM KCl, and then returned to contact sites within minutes after removal of this stimulus (Fig. 5 *A* and *B*, black lines, and Movie S2). Note that this dramatic redistribution of TMEM24 to the entire ER network confirms that peripheral TMEM24 patches reflects a localization of this protein in the ER, rather than in the PM. TMEM24 redistribution did not occur if cells were incubated with the cell-permeable Ca^{2+} chelator BAPTA-AM, indicating the dependence of this change on Ca^{2+} elevation in the cytosol (Fig. 5*B*, blue line). A similar dissociation of TMEM24 from the PM was observed upon depolarization induced by electric field stimulation, although a milder response occurred (Fig. 5*C*).

Another stimulus that induces Ca^{2+} influx into neurons is exposure to the excitatory neurotransmitter glutamate to activate ionotropic *N*-methyl-D-aspartate receptors (NMDARs). We tested the effect of bath application of 10 μM NMDA on neurons transiently expressing both TMEM24-EGFP and the intracellular Ca^{2+} probe R-GECO. Addition of NMDA induced a sharp increase in intracellular Ca^{2+} (Fig. 5 *E* and *–F*, red lines) concomitantly with the reversible loss of TMEM24-EGFP from peripheral patches (Fig. 5 *E* and *–F*, green lines). Both of these effects were abolished by the presence of the NMDAR-specific antagonist AP5 in the bath (Fig. 5*F*, blue and gray lines). To minimize the persistence of Ca^{2+} entry via the NMDARs, we coapplied an activity-dependent, noncompetitive antagonist MK801 with NMDA (33). Under these conditions, a brief surge in cytosolic Ca^{2+} (Fig. 5*F*, red line) was observed, which coincided with an equally transient loss of TMEM24-EGFP from ER–PM contact sites (Fig. 5*F*, green line). A second application of 10 μM NMDA elicited neither a Ca^{2+} response nor the dissociation of TMEM24-EGFP from the ER–PM contact sites, consistent with a block of NMDARs.

Transient partial dissociation of TMEM24-EGFP from ER–PM contacts was also observed upon spontaneously occurring Ca^{2+} spikes, indicating that such redistribution occurs under physiological conditions (Fig. 5*G*).

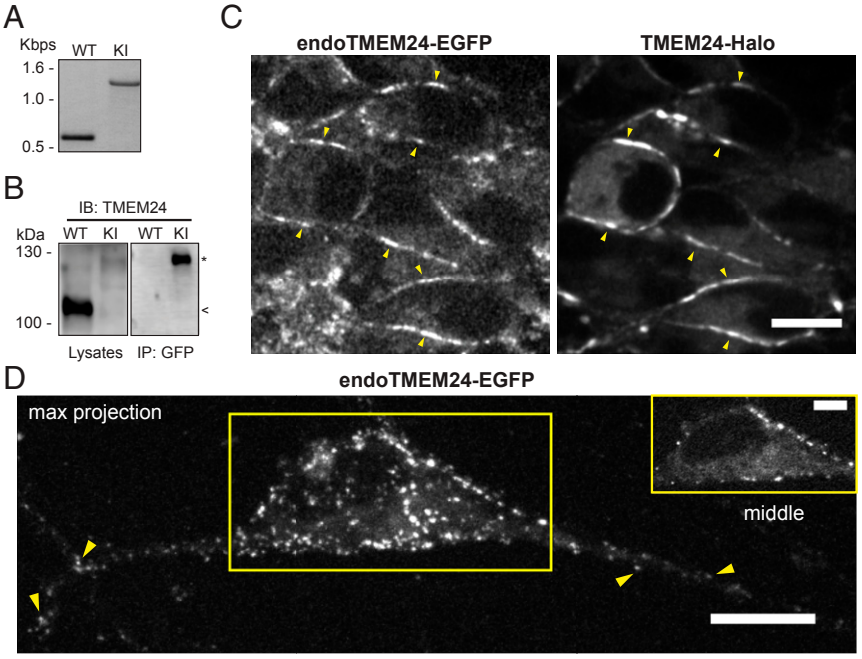

Fig. 4. TMEM24-EGFP expressed from the endogenous locus in human neuroblastoma cells localizes at ER–PM contact sites. (*A*) PCR amplification of a genomic segment comprising exon 14 and flanking sequences in WT and knockin (KI) IMR32 cells confirming the presence of the full EGFP donor sequence in the genomic DNA. (*B*) Anti-TMEM24 immunoblots (IB) of total lysates (*Left*) and of anti-GFP immunoprecipitates (IP) (*Right*) from WT and KI IMR32 cells. The WT TMEM24 band of control cells is replaced by a higher molecular weight band in knockin cells, which is highly enriched in the anti-GFP IP. Note the much lower intensity of the endo–TMEM24-EGFP band relative to the WT TMEM24 band. Arrowhead points to WT TMEM24 band. Asterisk points to endo–TMEM24-EGFP bands. (*C*) Representative confocal images of knockin IMR32 cells transfected with TMEM24-Halo. In cells expressing both proteins, TMEM24-Halo colocalizes with endo–TMEM24-EGFP in peripheral patches as indicated by arrowheads. (Scale bar, 10 μm.) (*D*) Maximum-intensity projection of a differentiated IMR32 cell (7 DIV) expressing endo–TMEM24-EGFP showing puncta of fluorescence both in the cell body and processes (as noted by yellow arrowheads). A single lower magnification equatorial plane image of the cell region enclosed by a rectangle (*Inset*) shows that the fluorescence signal has cortical localization. (Scale bar, 10 μm; 5 μm in *Inset*.)

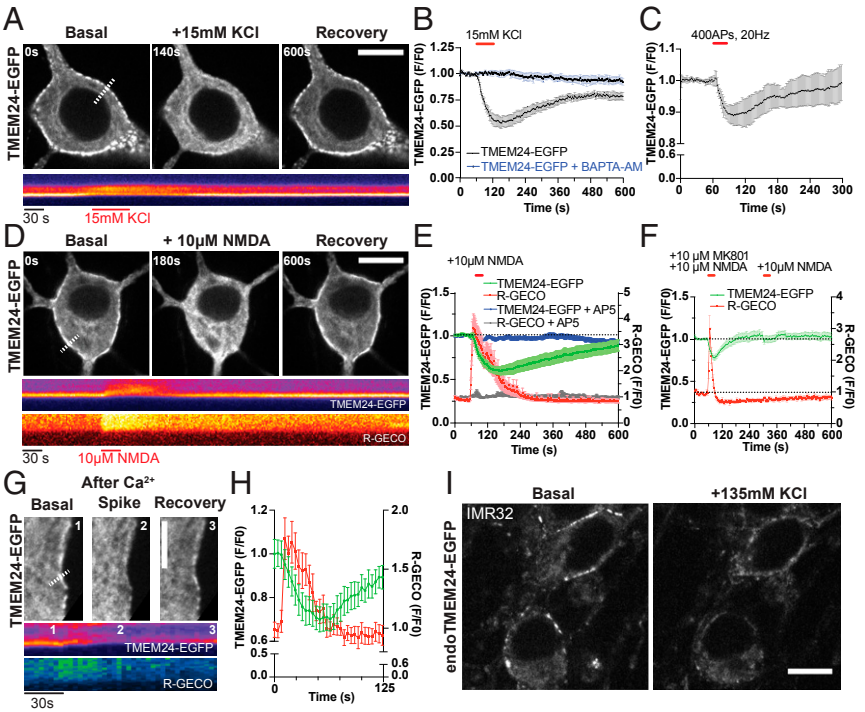

Fig. 5. Neuronal stimulation and spontaneous activity induce transient TMEM24 shedding from ER–PM contacts. (*A*) Confocal time course images of a cultured hippocampal neuron (13 DIV) transfected with TMEM24-EGFP showing a transient loss of the protein from ER–PM contacts upon acute exposure to 15 mM KCl (*Upper*). A kymograph of the dashed line is shown (*Lower*). (Scale bar, 10 μm.) (*B*) Quantification of *A* shown as the normalized fluorescence intensity of TMEM24-EGFP at ER–PM contact sites (black line). The transient dissociation of TMEM24-EGFP from the cortical ER is Ca^{2+}-dependent as the addition of the cell permeable Ca^{2+} chelator BAPTA-AM (10 μM), prevents it (blue line). Data are presented as mean ± SEM, $n = 8$ cells (−BAPTA-AM), $n = 14$ (+BAPTA-AM). (*C*) Quantification of normalized fluorescence intensity of transfected TMEM24-EGFP at ER–PM contact sites in cultured hippocampal neuron (14 DIV) following a field stimulation of 400 APs at 20 Hz (10 V), showing a transient dissociation of TMEM24 from the cortical ER. Data are presented as mean ± SD, $n = 5$ cells. (*D*) Confocal time-course images of cultured hippocampal neuron (15 DIV) transfected with TMEM24-EGFP showing its transient loss from ER–PM contact sites upon acute exposure to 10 μM NMDA (*Upper*). Kymographs of dashed line from both TMEM24-EGFP and the cytosolic Ca^{2+} indicator, R-GECO, are shown (*Lower*). (Scale bar, 10 μm.) (*E*) Quantification of *D* shown as the normalized fluorescence intensity of TMEM24-EGFP at ER–PM contact sites (green line) and the corresponding intracellular Ca^{2+} as indicated by R-GECO (red line). $n = 13$ cells. The addition of NMDAR antagonist, AP5, prevents both the transient dissociation of TMEM24-EGFP and the increase in intracellular $Ca2^{+}$ (blue and gray lines). $n = 13$ cells. All neurons are 13–15 DIV and all data are presented as mean ± SEM. (*F*) Quantification of normalized fluorescence intensity of transfected TMEM24-EGFP (green line) and R-GECO (red line) at ER–PM contact sites in cultured hippocampal neuron following NMDA treatments in the presence of the activity-dependent NMDAR inhibitor, MK801. Note that both Ca^{2+} and TMEM24-EGFP responses terminate faster than in the absence of MK801 (*E*) and that a second exposure to 10 μM NMDA evoked no response. All neurons are 11–13 DIV and all data are presented as mean ± SEM, $n = 12$ cells. (*G*) Confocal time-course images of the cortical region of a cultured hippocampal neuron (14 DIV) cotransfected with TMEM24-EGFP and R-GECO showing an example of spontaneously occurring transient loss of TMEM24-EGFP from ER–PM contact sites (*Upper*). Kymographs of the dashed line (*Lower*) show that this loss corresponds with a spontaneously occurring calcium spike. (Scale bar, 5 μm.) (*H*) Quantification of spontaneous events, like the one shown in *G*, aligned in the time axis by the peak in the Ca^{2+} spike. The normalized fluorescence intensities of R-GECO (red line) and of cortical TMEM24-EGFP (green line) are shown. All neurons are 13–14 DIV and data are presented as mean ± SEM, $n = 11$ cells. (*I*) Representative images of endo–TMEM24-EGFP in BrDu-differentiated (DIV 6) IMR32 cells. Upon treatment with 135 mM high KCl, the patchy peripheral fluorescence of endo–TMEM24-EGFP redistribute to internal fluorescence. (Scale bar, 10 μm.)

Finally, we found that elevation of cytosolic Ca^{2+} induced the dissociation of endo–TMEM24-EGFP from the PM in knockin IMR32 cells, further confirming that the PM-like signal of endo–TMEM24-EGFP represents ER signal and that the dynamic redistribution of TMEM24 occurs with the endogenous protein as well (Fig. 5*H*).

Phosphorylation Sites in the Polybasic CTR of TMEM24 Control Its Dissociation from ER–PM Contacts. We next investigated the molecular basis for the Ca^{2+}-regulated interaction of TMEM24 with the PM. As we had inferred from studies in nonneuronal cells, the localization of TMEM24 at ER–PM contact sites is mediated by a charged-based interaction of its positively charged CTR with anionic lipids in the cytosolic leaflet of the PM. We had also provided evidence for a role of PKC-dependent phosphorylation of TMEM24 in its Ca^{2+}-triggered dissociation from the PM (15). Inspection of TMEM24's CTR reveals polybasic clusters, the most prominent of which is localized at its C terminus. Deletion of 40 amino acids comprising this cluster (resulting in construct TMEM24-EGFP$^{1-666}$) (Fig. 6 *A*–*C*), or mutation of seven of the positive amino acids (K/Rs, indicated by blue asterisks in Fig. 6*A*) in this region to asparagine (TMEM24-EGFP^{7N}) abolished the enrichment of TMEM24-EGFP at ER–PM contacts relative to a luminal ER marker (RFP-KDEL), as shown by confocal microscopy analysis of live hippocampal neuronal cells (Fig. 6*D*). Interestingly, analysis of the CTR of TMEM24 using the NetPhos 3.1 server (www.cbs.dtu.dk/services/NetPhos/) revealed five serines with high score for potential PKC phosphorylation sites (confidence value >0.6) within its C-terminal polybasic patch (indicated in bold green fonts in Fig. 6*A*). A mutant TMEM24 in which all these five serines were replaced with the phosphomimetic amino acid glutamate (TMEM24-EGFP$^{5S\rightarrow E}$) (green stars in Fig. 6*A*) prevented ER–PM contact site localization (Fig. 6*E*). Conversely, replacing these five serines by the nonphosphorylatable amino acid asparagine (TMEM24-EGFP$^{5S\rightarrow N}$) was still localized at ER–PM contact sites when expressed in neurons (Fig. 6*F*). Importantly, however, this construct only showed a minimal dissociation from the ER–PM contact sites upon NMDA stimulation (Fig. 6*G*, black line) in contrast to the robust dissociation observed with the WT protein (Figs. 5*E* and 6*G*, green lines). We conclude that a phospho-switch involving the C terminus of TMEM24 plays the dominant role in the regulated dissociation of this protein from ER–PM contact sites. The minor dissociation still observed with TMEM24-EGFP$^{5S\rightarrow N}$ most likely reflects the presence of other phosphorylation sites for either PKC or other Ca^{2+}-regulated kinases present in the CTR.

TMEM24 Populates the Same Contacts as Kv2.1 Channels and VAP. Kv2.1 and Kv2.2, the major delayed rectifier K^{+} channels, are well-established components of ER–PM contacts in neurons (21, 34–36). As very recent studies have shown, these clusters are dependent on the interaction of a short amino acid sequence (an FFAT-like motif) in their CTR, with the MSP domain of VAP, a small protein of the ER membrane (25–27). In neuronal cultures, GFP-Kv2.1 clusters, like TMEM24-EGFP clusters, occur preferentially on the "basal" face of cells and often in ring-like

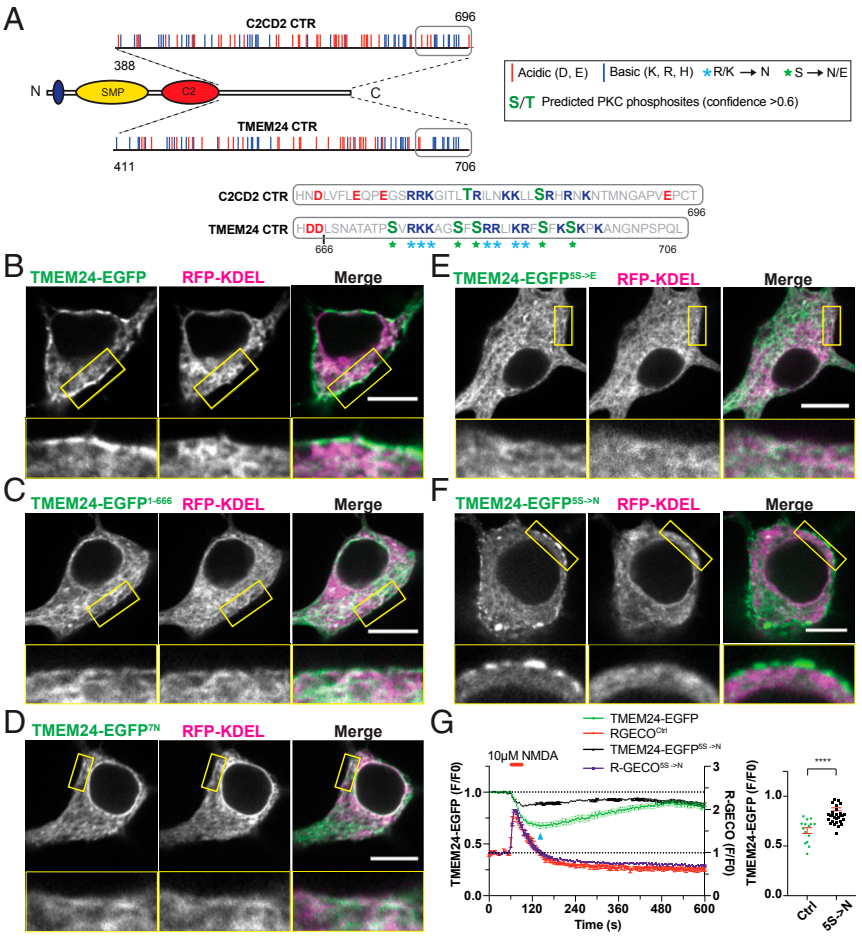

Fig. 6. Phosphorylation of the CTR is responsible for the dynamic regulation of TMEM24 at ER–PM contacts in neurons. (*A*) Schematic representation of the distribution of charged amino acid residues in the CTR of human TMEM24 and C2CD2. Basic residues (R/K) in TMEM24 used in mutagenesis experiments are indicated by blue asterisk. Serine residues with high confidence prediction for PKC phosphorylation (confidence value >0.6) according to the NetPhos 3.1 server and used in mutagenesis experiments are indicated by green stars. (*B–F*) Confocal images of cultured hippocampal neuron (10–13 DIV) cotransfected with WT or mutant TMEM24-EGFP constructs and with the ER luminal marker RFP-KDEL. *Insets* of the areas enclosed in rectangles are shown below the main images. TMEM24-EGFP partially colocalizes with the ER marker but is also enriched at the cortical ER (*B*). The TMEM24-EGFP$^{1–666}$ truncation mutant (*C*), the basic charge reduction TMEM24-EGFP$^{7R/K→N}$ mutant (*D*), and the phosphomimetic TMEM24-EGFP$^{5S→E}$ mutant (*E*) lose the enrichment in the cortical ER, while the nonphosphorylatable mutant TMEM24-EGFP$^{5S→N}$ (*F*) retains cortical ER localization. (Scale bar, 10 μm.) (Magnification: *B*, *C*, and *F Insets*, 2.5×; *D* and *E Insets*, 3.5×.) (*G*) Quantification of normalized fluorescence intensity of transfected WT TMEM24-EGFP (green line) or TMEM24-EGFP$^{5S→N}$ (black line) and R-GECO (red line) at ER-PM contact sites in cultured hippocampal neuron (10–13 DIV) following acute 10 μM NMDA application. Comparison of the time point indicated by arrowhead in the graph (*Left*) is shown in the scatter plot (*Right*). All data are presented as mean ± SEM, $n = 15$ cells (TMEM24-EGFP), $n = 28$ (TMEM24-EGFP$^{5S→N}$) [$t(41) = -7.16$, $^{****}P < 9.8 \times 10^{-9}$, two-tailed, unpaired *t* test].

shapes (21, 37), as described above for TMEM24 (Fig. S2). When both GFP-Kv2.1 and moderate levels of TMEM24-Halo were co-overexpressed together, they colocalized at the same cortical patches, as shown by both confocal microscopy (Fig. 7*A*) and total internal reflection fluorescence (TIRF) microscopy (*SI Appendix*, Fig. S4). VAP was also localized at the same sites (Fig. 7*B*). GFP-Kv2.1, however, which is known to be enriched at axon initial segments (38), was generally much more concentrated than TMEM24-Halo at patches in axon initial segments (Fig. 7). Upon high expression of TMEM24-Halo, GFP-Kv2.1 acquired a less clustered localization in cell bodies and dendrites (Fig. 7*C*). This was probably explained by the massively increased area of ER–PM apposition mediated by TMEM24 overexpression in cell bodies and dendrites, which allowed Kv2.1-VAP to disperse over a wider area. Clustering of Kv2.1 in the axon initial segment was less affected by TMEM24 overexpression, as TMEM24 is not enriched at these sites (Fig. 7*C*).

The TMEM24 Paralog C2CD2 Is also an ER–PM Tether but with Different Tissue Distribution and Regulation. TMEM24 has a paralog, C2CD2, which has the same domain organization (Fig. 1*A*) (12, 15). The two proteins share 29.8% overall sequence identity in humans with the greatest sequence similarity, besides their transmembrane domain, occurring in the CTR (Fig. 1*A*). C2CD2 and TMEM24, however, have very different tissue distribution (Fig. 1*B*). C2CD2 is barely detected in brain and is enriched in liver, with moderate expression levels in pancreatic islets and testis (Fig. 1*B*).

When expressed in the human hepatoma cell line Huh7, human C2CD2 fused to EGFP (C2CD2-EGFP) was enriched at cortical patches, but also colocalized throughout the cell with RFP-KDEL, consistent with a localization throughout the ER and an enrichment at ER–PM contact sites (Fig. 8*A*). As is the case of TMEM24, ER localization was dependent on its N-terminal region, which includes the putative transmembrane domain, as the removal of this region resulted in a cytosolic protein with an enrichment at the PM (Fig. 8*B*). Conversely, C2CD2 lacking its CTR was broadly localized in the ER without an enrichment at peripheral patches, consistent with a role of the CTR in PM binding (Fig. 8*C*), and speaking against a role of the C2 domain to such binding. Lack of a contribution of the C2 domain to membrane tethering for both TMEM24 (15) and C2CD2 was further confirmed by a liposome-based tethering assay. In this assay, cytosolic fragments of TMEM24 and C2CD2 comprising the short juxta-membrane region, the SMP and the C2 domain, but excluding the CTR, were "anchored" to ER-like liposomes [PC, DGS-NTA (Ni) and NBD-PE] via an N-terminal His-tag and mixed with PM-like liposomes [PC, phosphatidylserine (PS), PI(4,5)P_2]. No turbidity changes in the solution were observed upon addition of either protein, in the presence or absence of Ca^{2+}, indicating lack of tethering and aggregation (Fig. 8*D*). In contrast, the SMP-C2AB domains of E-Syt1, used as a positive control (39), efficiently tethered the liposomes in the presence of Ca^{2+}.

Despite the similarities between C2CD2 and TMEM24 in domain organization and protein localization, there was a difference in their response to Ca^{2+} elevation. In HeLa cells, TMEM24-EGFP dissociated from the PM when exposed to thapsigargin and then reassociated minutes later, as expected (15) (Fig. 8*E*, black line), whereas C2CD2-EGFP did not exhibit an obvious dissociation from the PM (Fig. 8*F*, black line). Similar differences

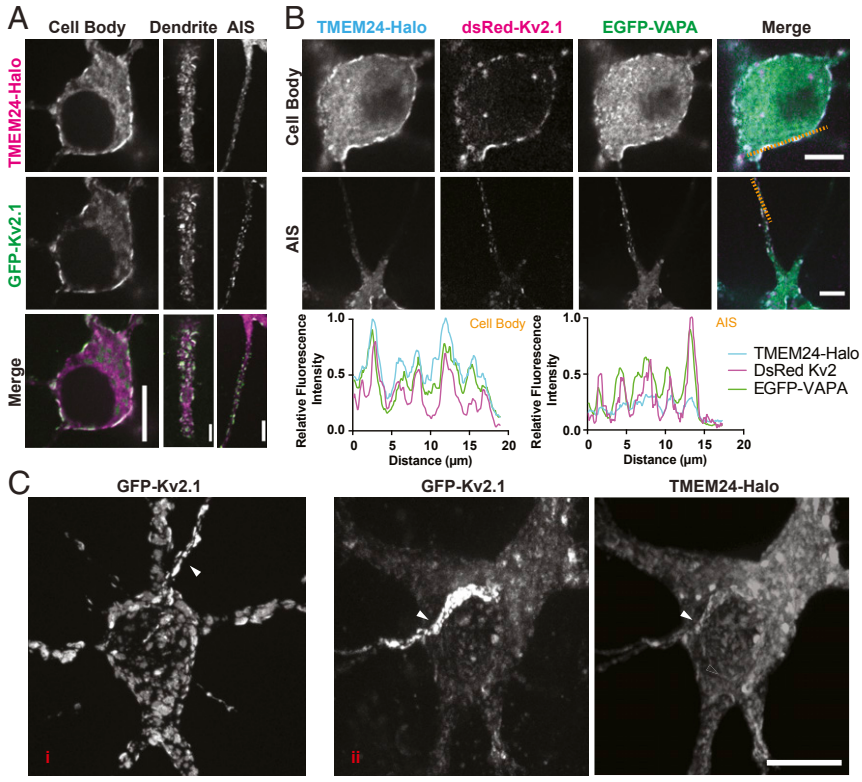

Fig. 7. Comparative analysis of the localization of TMEM24, Kv2.1, and VAP at ER–PM contact sites. Confocal images from cultured hippocampal neuron (10–14 DIV). (*A*) Confocal images showing colocalization of TMEM24-Halo and EGFP-Kv2.1 at cortical patches in cell bodies, dendrites, and axon initial segments (AIS). (Scale bars, 10 μm in cell body and 5 μm in dendrite and AIS.) (*B*) Confocal images of neurons cotransfected with TMEM24-Halo, DsRed-Kv2.1, and EGFP-VAPA showing that all three proteins colocalize at ER–PM contact sites. However, TMEM24-Halo is relatively less enriched than DsRed-Kv2.1 and EGFP-VAPA in the AIS. A cell body (*Top*) and an AIS (*Middle*) are shown. (Scale bars, *Top*, 10 μm; *Middle*, 5 μm.) Line scans of normalized relative fluorescence intensities along the indicated lines are shown (*Bottom*). (*C*) Representative maximum-intensity projections of confocal images of neurons transfected with EGFP-Kv2.1 alone (*i*) or both EGFP-Kv2.1 and TMEM24-Halo (*ii*). EGFP-Kv2.1 alone displays distinct PM clusters. These clusters become less distinct in cell body and dendrites upon the coexpression TMEM24-Halo while they remain very sharp and bright in the AIS (arrowhead) where EGFP-Kv2.1 is enriched relative to TMEM24-Halo. (Scale bar, 10 μm.)

in response to thapsigargin were observed when the CTRs of the two proteins were expressed alone (Fig. 8 *E* and *F*, blue lines). Both CTRs accumulated at the PM, but only the CTR of TMEM24 dissociated from the PM in response to thapsigargin.

We next compared the CTR of TMEM24 and C2CD2 for similarities and differences that could explain their shared property to concentrate at ER–PM contact sites, yet to be regulated differently. Similar polybasic clusters are present in the CTR of TMEM24 and C2CD2. However, only two residues (one serine and one threonine) that fit with a confidence value >0.6 the PKC consensus (www.cbs.dtu.dk/services/NetPhos/) are present in the C-terminal basic stretch of C2CD2, most likely explaining the different responses to thapsigargin.

Despite their overall difference in tissue distribution, both proteins can be detected together in some tissues (Fig. 1*B*). Because the SMP domain of TMEM24 dimerizes, and other SMP-containing proteins not only homodimerize (8, 15) but also heterodimerize (14) with their paralogs through their SMP domains, we investigated whether C2CD2 and TMEM24 can heterodimerize. The SMP domains of the two proteins were coexpressed in bacteria with His-SUMO and GST tags, respectively. Then, extracts of the bacteria were affinity-purified on a nickel resin to capture His-tagged C2CD2, and resin-bound complexes were eluted by cleaving the SUMO tag with SUMO protease. Eluted proteins were subsequently affinity-purified on glutathione beads to recover GST-TMEM24^{+} heterodimers. Size-exclusion chromatography of this material visualized by Coomassie blue staining demonstrated that both SMP domains coeluted in the same fractions at the expected molecular weight of the dimer (*SI Appendix*, Fig. S5), suggesting the occurrence of heterodimers in cells where both proteins are expressed.

Discussion

While the occurrence of contacts between the ER and the PM in neurons have been known for decades (18, 28, 40–42), only recently has a molecular inventory of proteins present at these sites started to be compiled. We report here that TMEM24, a lipid-transport protein preferentially expressed in neurons and in cells with neuron-like properties, is one component of such contacts and one whose localization is subject to regulation.

TMEM24 is localized at neuronal ER–PM contact sites at rest, and dissociates from the PM to redistribute throughout the entire ER upon perturbations that lead to a rise in cytosolic Ca^{2+}. This is shown in the present study both by exogenous expression of TMEM-EGFP in neurons or by adding an EGFP in frame to the endogenous *TMEM24* locus in human neuroblastoma cells. As shown previously, the interaction of TMEM24 with the PM is mediated by electrostatic interaction of its positively charged CTR with the negatively charged cytosolic leaflet of the PM, and is counteracted by PKC-dependent phosphorylation (15). Most likely PS at the PM, rather than $PI(4,5)P_2$ at this membrane, plays a major role in this interaction, as binding to the PM is not abolished by $PI(4,5)P_2$ dephosphorylation (15), a finding that we have confirmed. Accordingly, the CTR was identified in an unbiased screen for PS binding proteins (43). We have now found that a polybasic stretch in the CTR is the major determinant in

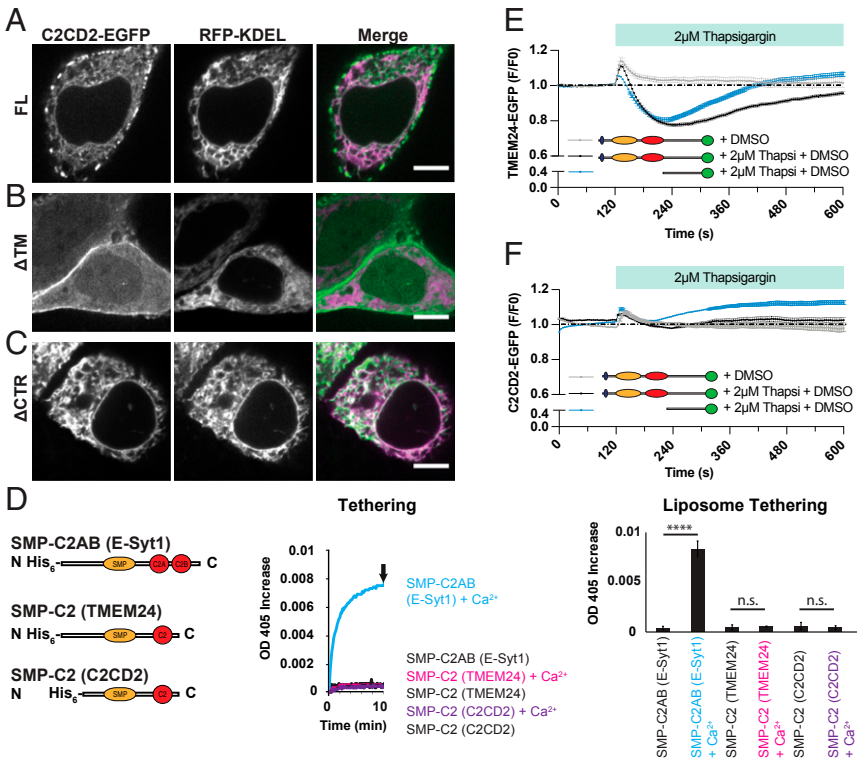

Fig. 8. Both TMEM24 and C2CD2 localize to ER–PM contact sites via their CTR but respond differently to Ca^{2+} elevation. (*A*–*C*) Representative confocal images of human hepatoma cells (Huh7) cotransfected with hC2CD2-EGFP constructs and the ER marker RFP-KDEL. (*A*) Full-length hC2CD2-EGFP partially colocalizes with the ER marker but is enriched at the cortical ER. (*B*) hC2CD2-EGFP without its transmembrane domain (ΔTM) decorates continuously the PM but also has a diffuse cytosolic localization. (*C*) hC2CD2-EGFP without its CTR (ΔCTR) localizes throughout the ER but is no longer enriched at the PM. (Scale bars, 10 μm.) (*D*) Liposome tethering assay. His tagged constructs of TMEM24 and C2CD2, as well as an His-E-Syt1 construct used as a control (*Left*) were anchored to ER-like (neutral phospholipids) liposomes via a DGS-NTA(Ni) lipid and incubated with PM-like [containing $PI(4,5)P_2$ and PS] liposomes. The curves (*Center*) demonstrate tethering of anchor and target liposomes as measured by the increase in turbidity (OD 405 nm) with or without Ca^{2+}. Bar graphs (*Right*) show OD 405 increase at the end of the incubation (arrow in *Center*). Data are represented as mean ± SEM $n = 3$, $^{****}P < 0.0001$, n.s. not significant (two-tailed, unpaired *t* test). (*E*) TIRF microscopy analysis of HeLa cells transfected with TMEM24-EGFP (black line) or its CTR-EGFP (blue line). Treatment with 2 μM thapsigargin, but not treatment with DMSO vehicle control (gray line), induces partial dissociation of TMEM24 and of the CTR from the PM followed by their recovery minutes later. All data are presented as mean ± SEM, $n = 38$–76 cells. (*F*) TIRF microscopy analysis of HeLa cells transfected with C2CD2-EGFP (black line) or its CTR-EGFP (blue line). Neither treatment with 2 μM thapsigargin nor DMSO vehicle control (gray line) induces appreciable changes in C2CD2 or its CTR alone from ER-PM. All data are presented as mean ± SEM, $n = 54$–62 cells.

PM association and showed the importance of several sites that fit the PKC consensus in this regulation.

A recent EM study of hippocampal neurons in culture demonstrated a reversible decrease in the area of ER–PM appositions within 30 s of high K^+ stimulation (44). The similar time course observed in our experiments for the shedding of TMEM24 from the PM raises the possibility that TMEM24 may be a determinant, or one of the determinants, of this structural rearrangement. Other ER proteins known to function as regulated tethers at ER–PM contact sites (e.g., E-Syt1 and STIM) are recruited rather than shed upon cell stimulation: E-Syt1 in response to cytosolic Ca^{2+} elevation (14, 45) and STIM1 in response to depletion of Ca^{2+} in the ER lumen (14, 31, 45). However, the specific contribution of these proteins as ER–PM tethers in neurons remains unclear. E-Syt1, in particular, whose Ca^{2+}-dependent recruitment to the PM shows nearly opposite dynamics relative to TMEM24 dissociation from this membrane when transfected in the same cell (46), is not expressed at high levels in brain (47) and analysis of brain single-cell genomics data reveals its preferential expression in non-neuronal cells (48).

A class of proteins that were recently shown to play a major role in the organization of ER–PM contacts in neurons are the PM-localized Kv2.1 and Kv2.2 channels (25, 26, 35). At rest, Kv2.1 and TMEM24 reside in the same contacts, although Kv2 channels are relatively more enriched than TMEM24 in ER–PM contacts at axon initial segments. The clustering of Kv2 channels at ER–PM contacts is dependent on their interaction with the ER protein VAP (25–27). VAP is a small tail-anchored protein of the ER membrane that serves as a multifunctional adaptor between the ER and a large variety of cytosolic proteins that contain the so-called FFAT motif (49, 50). Because VAP dimerizes and multimerizes, and many VAP binding proteins are lipid-metabolizing enzymes or lipid-transport proteins (49, 51), VAP may contribute, along with TMEM24, to coordinate the role of ER–PM contacts in ion transport and lipid dynamics. The Kv2–VAP interaction is also regulated by phosphorylation, but interestingly in a manner opposite to the regulation of the TMEM24–PM interaction (52, 53). Phosphorylation of serines within an atypical FFAT motif in the Kv2 channels confers to this peptide sequence the needed negative charge for fitting into the FFAT binding site of VAP (25, 26). Conversely, dephosphorylation of these serines promotes dissociation of the Kv2 channels from VAP and their dispersion throughout the PM (25, 26). Dispersion of Kv2 occurs in response to drastic perturbations, such as NMDAR stimulation and hypoxia (20, 52, 53), and over much longer time scales (minutes) than the rapid (tens of seconds), and rapidly reversible, dispersion of TMEM24 shown here.

It is of interest that another type of K^+ channel, the voltage and Ca^{2+}-regulated BK channels, localize at ER–PM contact sites in neurons (54, 55). While the mechanism underlying such

localization is not known, this would place them in close proximity of Ca^{2+} release sites from the ER, where the Ca^{2+}-release channel ryanodine receptors and IP3 receptors are localized. A concentration of PM localized Cav1.2 at the ER–PM was also reported (20). Thus, ER–PM contacts appear to be hubs where several ion channels are concentrated.

A key open question is the physiological function of TMEM24. The presence of an SMP domain in this protein and in vitro evidence for its lipid-transport properties (15) point to a role in lipid transport in vivo. A similar function has been demonstrated and proposed for other SMP domain-containing proteins localized at membrane contact sites (8, 9, 11, 12, 56). Mass spectrometry analysis revealed that the SMP domain of TMEM24 harbors glycerolipids, with a relative preference for inositol phospholipids (15). Because only low levels of phosphatidylinositol (PI) are present in the PM (56), this led to the suggestion that TMEM24 could function as a conduit for the delivery of newly synthesized PI from the ER to the PM at rest, to maintain appropriate pools of PI4P and PI(4,5)P_2. Conversely, its transient/reversible dissociation from the PM could help terminate stimulatory responses to signals that induce PI(4,5)P_2 hydrolysis by limiting the delivery of phosphatidylinositol for new PI(4,5)P_2 synthesis (15). This model remains to be further validated. It also cannot be excluded that TMEM24 may have a lipid-transport–independent function in vivo. For example, the head groups of phospholipids, which are expected to protrude from its hydrophobic cavity, may help form a binding interface for the regulation of other proteins.

TMEM24 has a paralogue, C2CD2, which is primarily expressed in nonneuronal tissues and has never been studied until now. Here we have shown that C2CD2 is also localized at ER–PM contact sites, although it is more resistant to dissociation from the PM in response to cytosolic Ca^{2+} elevation. The high sensitivity of TMEM24 to Ca^{2+} may be specially adapted to support the signaling functions of neurons and neuron-like cells.

Investigations of cells and organisms lacking expression of TMEM24 and C2CD2 will be critical to further elucidate the functions of these proteins. While studies of TMEM24 insulinoma knockout cells in vitro have shown defects in Ca^{2+} signaling and secretion, mice that we have generated that are knockout for TMEM24, C2CD2, or both proteins, are viable and fertile with no obvious major phenotypic defects. Thus, the physiological role of these proteins may be subtle, possibly overlapping with those of other lipid-transport proteins (57). We note that even mice that lack all three extended synaptotagmins are viable and fertile (47, 58). It would appear that there are many redundant pathways for the transport of lipids within cells so that the function of each specific pathway may be revealed only by specific perturbations.

Our findings add yet another protein to the repertoire of proteins localized at ER–PM contact sites in neurons. Not only close appositions between ER cisternae and the PM are abundant in neurons, but large ER cisterns with a narrow lumen and stapled to the PM are a special feature of many neurons or neuronal compartments in a subset of neurons (subsurface cisternae) (28, 40). The flurry of new information about proteins localized at ER–PM contacts (5, 6, 26, 59) is starting to yield insight into mechanisms that control these appositions and their potential physiological functions.

Collectively, studies of ER–PM contacts provide further evidence for an interplay between lipid signaling/metabolism and ion transport at the PM. Ion channels in the PM, including not only Kv2 channels but also other K^+ channels and Ca^{2+} channels, are generally positively regulated by their bilayer environment, by PI(4,5)P_2 in particular (60, 61). Conversely, ion channels in the PM control phospholipid metabolism by impacting enzymes of this metabolism, including PLC, through effects on cytosolic Ca^{2+} (62), either directly (Ca^{2+} channels) or indirectly (e.g., K^+ channels) via the control of membrane potential. The functional partnership between ion fluxes and lipid metabolism in the cross-talk between the PM and the ER, first appreciated through the discovery of the PLC/IP3/Ca^{2+} signaling pathway, is clearly more complex. Further exploration of this partnership will likely provide new insight into the control of neuronal signaling and excitability.

Materials and Methods

Antibodies and Chemicals. Rabbit anti-C2CD2 was generated by YenZym Antibody LLC using a C-terminal peptide from C2CD2 with the following sequence C-LNRKLLTRHRGKHTMNGVPRE. Rabbit anti-TMEM24 was previously described (15). GFP-Trap agarose beads were used for immunoprecipitation (ChromoTek), NMDA, AP-V, and MK801 (Tocris). Halo tag ligands JF549 and JF647 were a kind gift from L. Lavis, Janelia Farm, Ashburn, VA. All lipids were obtained from Avanti Polar Lipids. Sources of other antibodies and chemicals are listed in *SI Appendix, Supplemental Materials and Methods*.

Plasmids. Human C2CD2-EGFP in pReceiver M03 was purchased from GeneCopoeia and used as template to generate the truncated forms (ΔTMD and ΔCterm) by primer pairs 1 and 2 (*SI Appendix*, Table S1), respectively. TMEM24-EGFP and TMEM24-mCherry were previously described (15). See *SI Appendix, Supplemental Materials and Methods* for site-directed mutagenesis plasmids used and additional constructs used. Primers are listed in *SI Appendix*, Table S1

Primary Cultures of Brain Cells. All experiments involving mice were performed in accordance with the Yale University Institutional Animal Care and Use Committee. Primary cultures of hippocampi neurons were dissected from P0–P2 mouse brains, as previously described (15). See *SI Appendix, Supplemental Materials and Methods* for primary neuron and glial cell culture details.

Cell Line Culture and Transfection. HeLa cells (from ATCC) and human hepatoma Huh7 cells (kind gift of Michael Nathanson, Yale University, New Haven, CT) were cultured at 37 °C and 5% CO_2 in DMEM (Gibco Life Technology) containing 10% FBS, 1 mM sodium pyruvate, 100 U/mL penicillin, 100 mg/mL streptomycin, and 2 mM glutamax. IMR-32 were cultured at 37 °C and 5% CO_2 in RPMI containing 15% FBS, 1 mM sodium pyruvate, 100 U/mL penicillin, 100 mg/mL streptomycin, and 2 mM glutamax (all Gibco Life Technology). See *SI Appendix, Supplemental Materials and Methods* for IMR32 differentiation and transfection details.

Mouse Tissue/Organ Lysate Preparation. Multitissue lysates used for protein level analyses were obtained by homogenization of freshly collected tissues in ice-cold buffer containing 150 mM NaCl, 20 mM Hepes (Gibco Life Technology), pH 7.4, EDTA-free total protease inhibitor mixture (Roche), 0.5% SDS and Benzonase (Sigma-Aldrich). The total homogenate was placed on rotor at 4 °C for 30 min and centrifuged at 265,000 × *g* for 1 h at 4 °C. The supernatant was collected and kept on ice while a bicinchoninic acid assay (Thermo Fisher) was used to determine protein concentration. Proteins were separated using SDS/PAGE on 4–20% gel in Tris/glycine buffer (Bio-Rad). Protein gels were transferred onto nitrocellulose membrane for immunoblotting.

Live Cell Imaging. Primary neuronal cells were gently washed and incubated at 33–37 °C in the following buffer containing: 137 mM NaCl, 5 mM KCl, 2 mM $CaCl_2$, 1 mM $MgCl_2$, 30 mM D-glucose, 10 mM Hepes with pH adjusted to 7.4 with NaOH. For all HeLa and Huh7 cells experiments the buffer contained: 125 mM NaCl, 5 mM KCl, 1.3 mM $CaCl_2$, 1.2 mM $MgCl_2$, 3 mM D-glucose, 10 mM Hepes adjusted to PH 7.4 with NaOH. Images were sampled at 0.25 Hz. See *SI Appendix, Supplemental Materials and Methods* for specific experimental and microscope specifications.

Liposome Tethering Assays. Human E-Syt1$_{SMP\text{-}C2AB}$ (residues 93–634) was amplified by PCR and cloned using AscI and NotI sites into the pCMV6-An-His vector (Origene) for Expi293 cell expression. Human TMEM24$_{SMP\text{-}C2}$ (36-414) and C2CD2$_{SMP\text{-}C2}$ (39-405) were cloned using NheI and XhoI sites into pET-28a vector (Novagen).

ACKNOWLEDGMENTS. We thank L. Benedetti, S. Gowrishankar, A. J. McCartney, and J. Lees for discussion; F. Wilson, H. Wheeler, L. J. Liu, R. Coolon, L. Lucast, and S. Wilson for outstanding technical assistance; X. J. Zhao, R. Cardone, and R. Kibbey (Diabetes Center, Yale University) for providing mouse pancreatic islets; E. Kruglov (Liver Center, Yale University) for providing Huh7 cells; James Trimmer (University of California, Davis) for discussion and advice; and James Trimmer, Joerg Bewersdorf, James Rothman, and Karin Reinisch (Yale University) for donating critical reagents. This work was supported by National

Institutes of Health Grants NS36251, DA018343, and DK45735 (to P.D.C.); and a grant from the Kavli Foundation (to P.D.C.). X.B. was supported by a Human Frontier Science Program long-term postdoctoral fellowship; and E.W.S. was supported in part from the NIH predoctoral program in Cellular and Molecular Biology (T32 GM007223) and the NIH T32 Neurobiology of Cortical Systems Training grant. A.G.S. was supported by the Gruber Science Fellowship.

1. Wirtz KW (1991) Phospholipid transfer proteins. *Annu Rev Biochem* 60:73–99.
2. Drin G (2014) Topological regulation of lipid balance in cells. *Annu Rev Biochem* 83: 51–77.
3. Holthuis JCM, Menon AK (2014) Lipid landscapes and pipelines in membrane homeostasis. *Nature* 510:48–57.
4. Prinz WA (2014) Bridging the gap: Membrane contact sites in signaling, metabolism, and organelle dynamics. *J Cell Biol* 205:759–769.
5. Saheki Y, De Camilli P (2017) Endoplasmic reticulum-plasma membrane contact sites. *Annu Rev Biochem* 86:659–684.
6. Gallo A, Vannier C, Galli T (2016) Endoplasmic reticulum-plasma membrane associations: Structures and functions. *Annu Rev Cell Dev Biol* 32:279–301.
7. Levine T, Loewen C (2006) Inter-organelle membrane contact sites: Through a glass, darkly. *Curr Opin Cell Biol* 18:371–378.
8. Schauder CM, et al. (2014) Structure of a lipid-bound extended synaptotagmin indicates a role in lipid transfer. *Nature* 510:552–555.
9. Toulmay A, Prinz WA (2012) A conserved membrane-binding domain targets proteins to organelle contact sites. *J Cell Sci* 125:49–58.
10. Wong LH, Levine TP (2017) Tubular lipid binding proteins (TULIPs) growing everywhere. *Biochim Biophys Acta Mol Cell Res* 1864:1439–1449.
11. Kawano S, et al. (2017) Structure-function insights into direct lipid transfer between membranes by Mmm1-Mdm12 of ERMES. *J Cell Biol* 217:959–974.
12. Alva V, Lupas AN (2016) The TULIP superfamily of eukaryotic lipid-binding proteins as a mediator of lipid sensing and transport. *Biochim Biophys Acta* 1861:913–923.
13. Kornmann B, et al. (2009) An ER-mitochondria tethering complex revealed by a synthetic biology screen. *Science* 325:477–481.
14. Giordano F, et al. (2013) PI(4,5)P_2-dependent and $Ca^{(2+)}$-regulated ER-PM interactions mediated by the extended synaptotagmins. *Cell* 153:1494–1509.
15. Lees JA, et al. (2017) Lipid transport by TMEM24 at ER-plasma membrane contacts regulates pulsatile insulin secretion. *Science* 355:eaah6171.
16. Liu L-K, Choudhary V, Toulmay A, Prinz WA (2017) An inducible ER-Golgi tether facilitates ceramide transport to alleviate lipotoxicity. *J Cell Biol* 216:131–147.
17. Pottekat A, et al. (2013) Insulin biosynthetic interaction network component, TMEM24, facilitates insulin reserve pool release. *Cell Rep* 4:921–930.
18. Henkart M, Landis DM, Reese TS (1976) Similarity of junctions between plasma membranes and endoplasmic reticulum in muscle and neurons. *J Cell Biol* 70:338–347.
19. Lim ST, Antonucci DE, Scannevin RH, Trimmer JS (2000) A novel targeting signal for proximal clustering of the Kv2.1 K+ channel in hippocampal neurons. *Neuron* 25: 385–397.
20. Fox PD, et al. (2015) Induction of stable ER-plasma-membrane junctions by Kv2.1 potassium channels. *J Cell Sci* 128:2096–2105.
21. Antonucci DE, Lim ST, Vassanelli S, Trimmer JS (2001) Dynamic localization and clustering of dendritic Kv2.1 voltage-dependent potassium channels in developing hippocampal neurons. *Neuroscience* 108:69–81.
22. Kakizawa S, Moriguchi S, Ikeda A, Iino M, Takeshima H (2008) Functional crosstalk between cell-surface and intracellular channels mediated by junctophilins essential for neuronal functions. *Cerebellum* 7:385–391.
23. Kraft R (2015) STIM and ORAI proteins in the nervous system. *Channels (Austin)* 9: 245–252.
24. de Juan-Sanz J, et al. (2017) Axonal endoplasmic reticulum Ca^{2+} content controls release probability in CNS nerve terminals. *Neuron* 93:867–881.e6.
25. Johnson B, et al. (2018) Kv2 potassium channels form endoplasmic reticulum/plasma membrane junctions via interaction with VAPA and VAPB. *Proc Natl Acad Sci USA* 115: E7331–E7340.
26. Kirmiz M, Vierra NC, Palacio S, Trimmer JS (2018) Identification of VAPA and VAPB as Kv2 channel-interacting proteins defining endoplasmic reticulum-plasma membrane junctions in mammalian brain neurons. *J Neurosci* 38:7562–7584.
27. Sun EW, De Camilli P (2018) Kv2 potassium channels meet VAP. *Proc Natl Acad Sci USA* 115:7849–7851.
28. Wu Y, et al. (2017) Contacts between the endoplasmic reticulum and other membranes in neurons. *Proc Natl Acad Sci USA* 114:E4859–E4867.
29. Los GV, et al. (2008) HaloTag: A novel protein labeling technology for cell imaging and protein analysis. *ACS Chem Biol* 3:373–382.
30. Sher E, Denis-Donini S, Zanini A, Bisiani C, Clementi F (1989) Human neuroblastoma cells acquire regulated secretory properties and different sensitivity to Ca2+ and alpha-latrotoxin after exposure to differentiating agents. *J Cell Biol* 108:2291–2300.
31. Liou J, et al. (2005) STIM is a Ca2+ sensor essential for Ca2+-store-depletion-triggered Ca2+ influx. *Curr Biol* 15:1235–1241.
32. Kobayashi S, Kitazawa T, Somlyo AV, Somlyo AP (1989) Cytosolic heparin inhibits muscarinic and alpha-adrenergic Ca2+ release in smooth muscle. Physiological role of inositol 1,4,5-trisphosphate in pharmacomechanical coupling. *J Biol Chem* 264: 17997–18004.
33. Song X, et al. (2018) Mechanism of NMDA receptor channel block by MK-801 and memantine. *Nature* 556:515–519.
34. Mandikian D, et al. (2014) Cell type-specific spatial and functional coupling between mammalian brain Kv2.1 K+ channels and ryanodine receptors. *J Comp Neurol* 522: 3555–3574.
35. Du J, Tao-Cheng JH, Zerfas P, McBain CJ (1998) The K+ channel, Kv2.1, is apposed to astrocytic processes and is associated with inhibitory postsynaptic membranes in hippocampal and cortical principal neurons and inhibitory interneurons. *Neuroscience* 84: 37–48.
36. Fox PD, et al. (2013) Plasma membrane domains enriched in cortical endoplasmic reticulum function as membrane protein trafficking hubs. *Mol Biol Cell* 24:2703–2713.
37. Zhang Y, McKay SE, Bewley B, Kaczmarek LK (2008) Repetitive firing triggers clustering of Kv2.1 potassium channels in Aplysia neurons. *J Biol Chem* 283:10632–10641.
38. Sarmiere PD, Weigle CM, Tamkun MM (2008) The Kv2.1 K+ channel targets to the axon initial segment of hippocampal and cortical neurons in culture and in situ. *BMC Neurosci* 9:112.
39. Bian X, Saheki Y, De Camilli P (2018) Ca^{2+} releases E-Syt1 autoinhibition to couple ER-plasma membrane tethering with lipid transport. *EMBO J* 37:219–234.
40. Rosenbluth J (1962) Subsurface cisterns and their relationship to the neuronal plasma membrane. *J Cell Biol* 13:405–421.
41. Smith CA, Sjostrand FS (1961) Structure of the nerve endings on the external hair cells of the Guinea pig cochlea as studied by serial sections. *J Ultrastruct Res* 5:523–556.
42. Wu Y, et al. (2014) A dynamin 1-, dynamin 3- and clathrin-independent pathway of synaptic vesicle recycling mediated by bulk endocytosis. *eLife* 3:e01621.
43. Caberoy NB, Zhou Y, Alvarado G, Fan X, Li W (2009) Efficient identification of phosphatidylserine-binding proteins by ORF phage display. *Biochem Biophys Res Commun* 386:197–201.
44. Tao-Cheng J-H (2018) Activity-dependent decrease in contact areas between subsurface cisterns and plasma membrane of hippocampal neurons. *Mol Brain* 11:23.
45. Idevall-Hagren O, Lü A, Xie B, De Camilli P (2015) Triggered Ca2+ influx is required for extended synaptotagmin 1-induced ER-plasma membrane tethering. *EMBO J* 34: 2291–2305.
46. Xie B, Nguyen PM, Idevall-Hagren O (December 27, 2018) Feedback regulation of insulin secretion by extended synaptotagmin-1. *FASEB J*, 10.1096/fj.201801878R.
47. Herdman C, Tremblay MG, Mishra PK, Moss T (2014) Loss of extended synaptotagmins ESyt2 and ESyt3 does not affect mouse development or viability, but in vitro cell migration and survival under stress are affected. *Cell Cycle* 13:2616–2625.
48. Macosko EZ, et al. (2015) Highly parallel genome-wide expression profiling of individual cells using nanoliter droplets. *Cell* 161:1202–1214.
49. Murphy SE, Levine TP (2016) VAP, a versatile access point for the endoplasmic reticulum: Review and analysis of FFAT-like motifs in the VAPome. *Biochim Biophys Acta* 1861:952–961.
50. Huttlin EL, et al. (2015) The BioPlex network: A systematic exploration of the human interactome. *Cell* 162:425–440.
51. Kaiser SE, et al. (2005) Structural basis of FFAT motif-mediated ER targeting. *Structure* 13:1035–1045.
52. Misonou H, et al. (2004) Regulation of ion channel localization and phosphorylation by neuronal activity. *Nat Neurosci* 7:711–718.
53. Misonou H, Mohapatra DP, Menegola M, Trimmer JS (2005) Calcium- and metabolic state-dependent modulation of the voltage-dependent Kv2.1 channel regulates neuronal excitability in response to ischemia. *J Neurosci* 25:11184–11193.
54. Kaufmann WA, et al. (2009) Large-conductance calcium-activated potassium channels in Purkinje cell plasma membranes are clustered at sites of hypolemmal microdomains. *J Comp Neurol* 515:215–230.
55. Irie T, Trussell LO (2017) Double-nanodomain coupling of calcium channels, ryanodine receptors, and BK channels controls the generation of burst firing. *Neuron* 96: 856–870.e4.
56. Saheki Y, et al. (2016) Control of plasma membrane lipid homeostasis by the extended synaptotagmins. *Nat Cell Biol* 18:504–515.
57. Nimitvilai S, et al. (2017) Orbitofrontal neuroadaptations and cross-species synaptic biomarkers in heavy-drinking macaques. *J Neurosci* 37:3646–3660.
58. Sclip A, Bacaj T, Giam LR, Südhof TC (2016) Extended synaptotagmin (ESyt) triple knock-out mice are viable and fertile without obvious endoplasmic reticulum dysfunction. *PLoS One* 11:e0158295.
59. Phillips MC, Johnson WJ, Rothblat GH (1987) Mechanisms and consequences of cellular cholesterol exchange and transfer. *Biochim Biophys Acta* 906:223–276.
60. Suh B-C, Hille B (2008) PIP2 is a necessary cofactor for ion channel function: How and why? *Annu Rev Biophys* 37:175–195.
61. Huang CL, Feng S, Hilgemann DW (1998) Direct activation of inward rectifier potassium channels by PIP2 and its stabilization by Gbetagamma. *Nature* 391:803–806.
62. Putney JW, Tomita T (2012) Phospholipase C signaling and calcium influx. *Adv Biol Regul* 52:152–164.